Electrical Impedance Tomography in 3D using two electrode planes: characterization and evaluation

Justin Wagenaar[1], **Andy Adler**[1]

[1]Systems and Computer Engineering, Carleton University, Ottawa, Canada

Abstract. Electrical Impedance Tomography (EIT) uses body surface electrical stimulation and measurements to create conductivity images; it shows promise as a non-invasive technology to monitor the distribution of lung ventilation. Most applications of EIT have placed electrodes in a 2D ring around the thorax, and thus produced 2D cross-sectional images. These images are unable to distinguish out-of-plane contributions, or to image volumetric effects. Volumetric EIT can be calculated using multiple electrode planes and a 3D reconstruction algorithm. However, while 3D reconstruction algorithms are available, little has been done to understand the performance of 3D EIT in terms of the measurement configurations available. The goal of this paper is to characterize the phantom and in vivo performance of 3D EIT with two electrode planes. First, phantom measurements are used to measure the reconstruction characteristics of seven stimulation and measurement configurations. Measurements were then performed on eight healthy volunteers as a function of body posture, postures, and with various electrode configurations. Phantom results indicate that 3D EIT using two rings of electrodes provides reasonable resolution in the electrode plane but low vertical resolution. For volunteers, functional EIT images are created from inhalation curve features to analyze the effect of posture (standing, sitting, supine and decline) on regional lung behaviour with the greater lung. An ability to detect vertical changes in lung volume distribution was shown for two electrode configurations. Based on tank and volunteer results, we recommend the use of the "Square" stimulation and measurement pattern for two electrode plane EIT.

Keywords: Electrical Impedance Tomography, 3D Lung Imaging Image Reconstruction

1. Introduction

Electrical Impedance Tomography (EIT) is an imaging approach which seeks to calculate a conductivity map of the interior of a body from the application of patterns of AC currents and recording of voltage surface measurements on a set of electrodes placed on the body surface. EIT is sensitive to conductivity contrasting fluids and gases, and thus shows promise for monitoring blood flow and breathing in the thorax.

Because of the diffusive nature of current flow in a body, the physics of EIT is inherently a three dimensional. The most common application of EIT has been using electrodes placed in an single transverse plane, and reconstructing onto a 2D image "slice". This planar simplification is most common in chest EIT and in many

geophysical and process tomography applications; in EIT of the breast and brain non-planar electrode placements are more common. In the early stages of EIT research, the computational requirements in processing power and memory for 3D reconstruction were large; currently, advances in computer hardware mean this is no longer true.

However, even when the reconstruction problem is formulated using a 3D sensitivity matrix, there are inherent limitations to restricting the problem to a planar one. First, the 2D EIT image is not a "slice" but rather is sensitive to large volume. This region of sensitivity has been described as a "lens shaped" region extending to $\frac{1}{2}$ of the body diameter above and below the electrode plane (Putensen *et al* 2006). However the shape of the sensitive region depends also on many other factors, such as the current stimulation pattern and the presence of conductivity contrasting lungs (Adler *et al* 2015). Additionally, interpretation of a EIT image as slice requires an assumption that inhomogeneities occur only in the image plane and thus that the image is uniform in the out-of-plane (cranial-caudal) direction. For lung EIT, this assumption may often be legitimate for lung injury, but is less reasonable for highly heterogeneous obstructive lung diseases (for example, as shown by Kirby *et al* (2011) using hyperpolarized He MRI). For such heterogeneous conditions, regions in 2D EIT images would represent a conflation of various contrasts in the volume. In these cases, 3D imaging has the potential to improve distinguishability to adding volumetric resolution.

Many 3D reconstruction approaches have been proposed, starting in medical EIT with Metherall *et al* (1996). An open sourced software package including 3D reconstruction tools has been released (Polydorides & Lionheart, 2002) and work has been done to evaluate new 3D reconstruction approaches (Stephenson *et al* 2005). However, there has been relatively little consideration put towards the appropriate selection of stimulation and measurement patterns for 3D EIT. Even with two planes, the variety of spatial patterns is much larger than for a single plane.

Most available EIT systems make stimulations and measurement between pairs of electrodes, mostly because of this configuration allows improved electronics performance. The most common configuration in medical EIT is the Sheffield (or Adjacent) stimulation and measurement pattern. With a planar electrode placement, using a pair-drive EIT system, stimulation and measurement patterns are characterized by a "skip" — the number of electrodes between those in each stimulation or measurement pair. An adjacent drive system uses "skip 0", while an 16-electrode opposite drive system uses "skip 7".

On the other hand, a 3D placement of electrodes, even with only two rings, allows far variety of patterns. The selection of the measurement protocol would be expected to have significant impact on image quality and robustness.

In general it is possible to use an EIT system designed for adjacent stimulation and measurements in many other configurations by the simple rearrangement of electrodes, by which any skip pattern relatively prime to the number of electrodes can be achieved (Mamatjan *et al* 2011). This possibility is the main motivation for our study: given one of the pair-drive EIT systems available today, how can its electrodes be best rearranged

into a 3D configuration?

The main work toward evaluation of 3D stimulation and measurement patterns was by Graham & Adler (2007), which simulated a cylindrical tank phantom and evaluated seven proposed measurement patterns based on a two-ring arrangement. Results showed a range of performance trends over a number of different image quality parameters, with the "Planar" electrode placement pattern being the strongest performer. These seven patterns were explored further in (Mamatjan *et al* 2011) using a "distinguishability" criterion, and the "Zigzag-Interleaved" pattern showed best overall performance.

Several studies evaluated novel 3D electrode measurement patterns for breast and brain imaging. Deghani *et al* (2005), used SVD analysis of the Jacobian matrix to compare information content in different excitation configurations using a voltage drive system, in which out-of-phase electrode planes gave the highest performance. Another study Fabrizi *et al* (2009) used empirical data from a semi-spherical phantom to evaluate 10 3D measurement protocols with varying current injection combinations to determine an optimal pattern. Additionally, Kantartzis *et al* (2013) developed stability measure for breast imaging, which was used to show that little improvement was seen by varying electrode distributions and that increasing the number of electrodes in the stimulation group led to a step-wise increase in performance. However the majority of available EIT devices still use the standard electrode pair current drive pattern (Adler *et al* 2011) and as such an evaluation under the system restraints of this pattern is useful.

In this work, we take this evaluation one step further, and perform the evaluation on tank phantoms and human volunteers using a standard Sheffield current pattern configuration. We seek to validate whether the simulation results continue to be valid, and to determine what kinds of practical interference occur.

2. Methods

Our goal was to better understand the effects of 3D measurement patterns on the quality of reconstructed images. First, simulation results from previous works were repeated, and used to guide the design of tank phantom experiments. Based on these results, the best measurement patterns were used in human volunteer tests. In these tests, regional lung mechanics were varied in the vertical direction by taking EIT recordings of subjects while breathing in different postures: standing, sitting, supine, and decline.

This study compared the seven measurement patterns developed by Graham & Adler (2007), shown in Figure 1. These patterns were designed to use standard EIT designed for adjacent measurement and varying the electrode placement. They were named: Planar (PL), Planar Offset (PO), Planar Opposite (PP), Zigzag (ZZ), Zigzag Offset (ZO), Zigzag Opposite (ZP), and Square (SQ). Our approach to evaluate each pattern is outlined in the Figure 2, for the tank phantom and human volunteer studies.

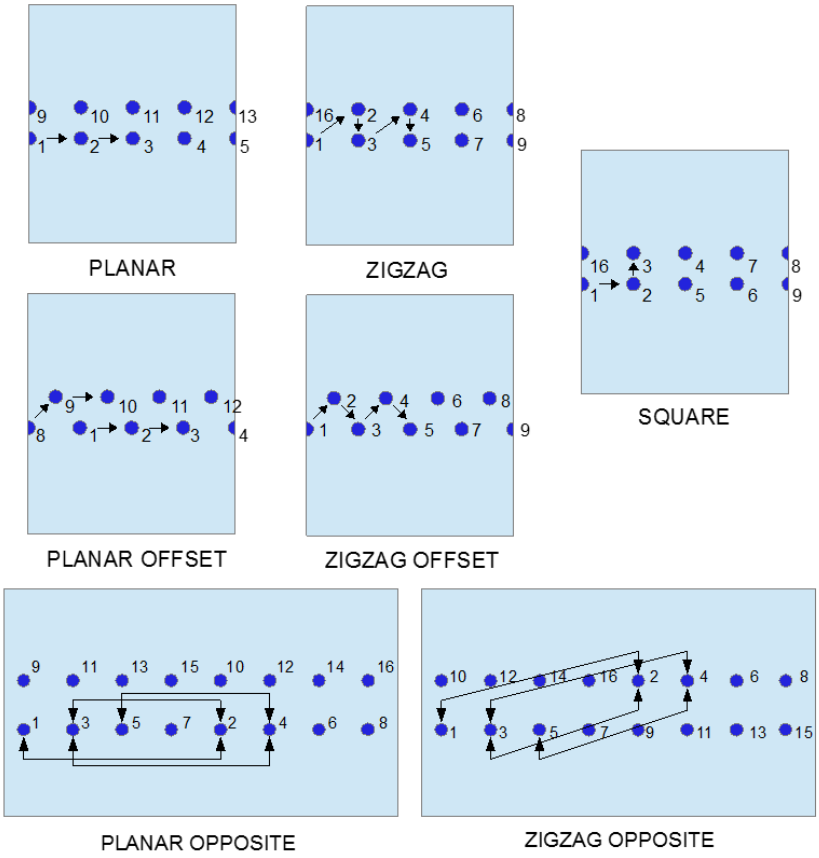

Figure 1: Electrode placement patterns developed in (Graham & Adler, 2007) consisting of two rings of both aligned and offset patterns.

2.1. Image Reconstruction

Image reconstruction in this paper was performed using the 3D GREIT method (Grychtol *et al* 2015), which is described in (Grychtol *et al* 2015). Briefly, reconstruction can be developed from a forward problem, $v = F(\sigma)$, where v is a vector of the set of measurements in an EIT frame, and σ is a vector of the discretized conductivity. $F(\cdot)$ describes the generation of measurements, typically using a finite element model, and n describes a vector of noise in the system. For time-difference EIT, we consider the change in measurements $y = Jx + n$, where $y = v - v_0$ is the difference between current measurements and those at some reference time v_0. Similarly the conductivity difference is given by $x = \sigma - \sigma_0$, and J is a sensitivity matrix which relates the change in conductivity to the change in measurement.

The GREIT approach calculates a reconstruction matrix, R, which is best over a "training" set of measurements and images. This optimization seeks to minimize

$$\sum_i w_i \|t_i - Ry_i\|^2 \tag{1}$$

where t_i is the "desired image" which corresponds to training measurement frame y_i,

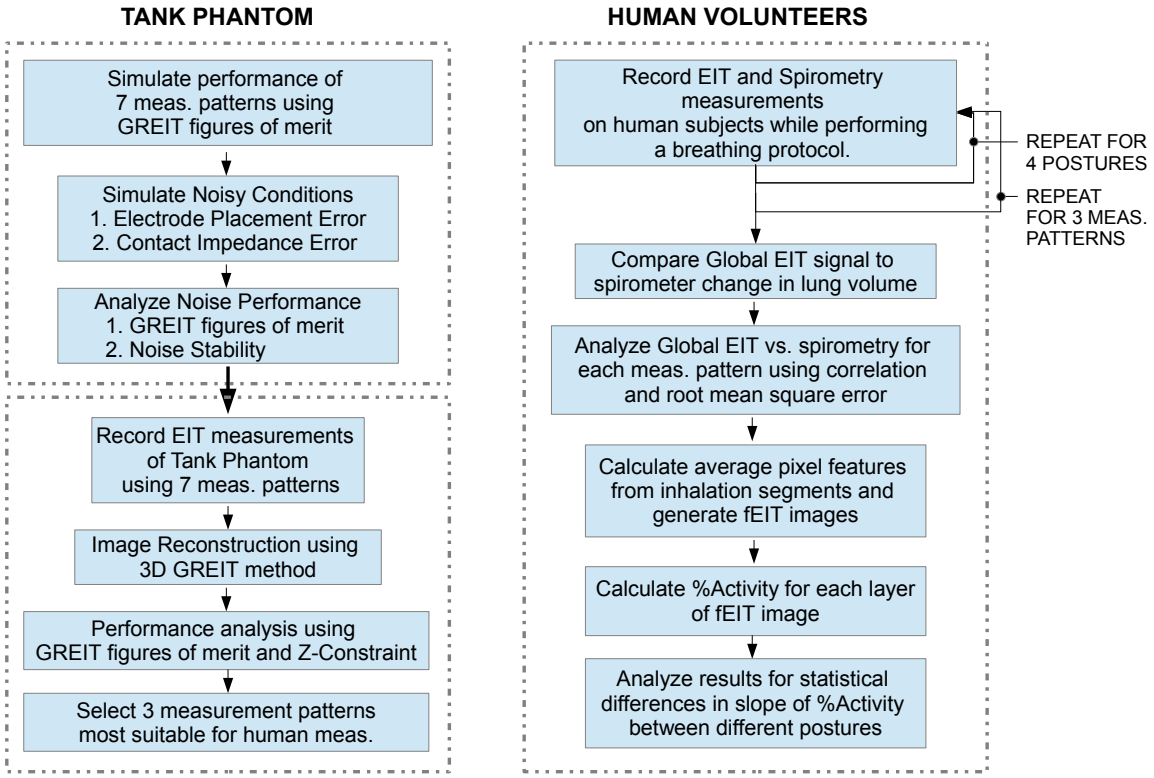

Figure 2: Block diagram of characterization and evaluation aproach.

and w_i is a weighting of the "importance" of i in the calculation of R. Solving (1) yields

$$R = \left(\sum_i w_i t_i y_i^T \right) \left(\sum_i w_i y_i y_i^T + \lambda^2 \Sigma_n \right)^{-1} \tag{2}$$

where Σ_n is the covariance of the system noise, and λ is a parameter which determined the noise performance of the reconstruction; its value is found by bisection search until the requested noise figure is obtained.

In the formulation of the GREIT algorithm (Adler *et al* 2009), a set of consensus figures of merit were presented which drive the choice of t_i and y_i. The reconstruction matrix is calculated such that the reconstructed target images have both the desired image quality and noise performance. The GREIT method has been extended to a 3D algorithm by extending the target set to cover a 3D space and reconstructing onto a 3D reconstruction model (Wagenaar *et al* 2014, Grychtol *et al* 2015).

2.2. Simulations

Simulations were performed to analyze the performance of the seven measurement patterns under clean and noisy conditions in order to establish baseline performance trends. Sources of noise considered here to be most relevant to lung imaging were

electrode placement error and contact impedance error. Simulations were processed using EIDORS v.3.8 available from `eidors.org` (Adler & Lionheart, 2006). Simulation results were analyzed using the GREIT figures of merit (FoM), and are available in the thesis describing this work (Wagenaar, 2015). Results agreed with previous results presented by Graham & Adler (2007), and are therefore not discussed further here. The PL and PO patterns showed the best overall noise performance but with lower performance at the edges of the model. The ZZ, ZO and SQ patterns were especially susceptible to electrode placement error. Both the ZP and PP patterns were very susceptible to noise and produced poor results.

2.3. Tank Measurements

A phantom tank experiment was performed to evaluate the performance of the seven 3D measurement patterns using measured data and compare with simulated results, and to select the three best-suited measurement patterns to be used in the Human Measurements experiment described in the following chapter.

A cylindrical saline phantom was used with 14 cm radius and 36 cm height and equipped with 4 rows of 32 electrodes. A non-conductive plastic cube of 50 ml was used as the target for this test. The block was placed at 15 different positions within the tank as shown in Figure 3 and EIT measurements were made using the seven measurement patterns. Measurements were taken using the GOE-MF II (Carefusion, Höchberg, Germany) device. This device uses an adjacent stimulation and measurement pattern. In order to implement different patterns, the electrode connector cables were moved and attached to the corresponding locations. Images were reconstructed on a cylindrical finite element model (FEM) and the performance of the patterns were evaluated using the GREIT parameters which describe planar characteristics.

In order to measure the vertical resolution in reconstructed images, we define the "Z-Resolution" as the half-maximum width of the reconstructed image in the z-axis. As shown in figure 4, the Z-Resolution is defined as the distance between the upper and lower half-maximum layer pixel amplitude points normalized over the cylinder height. The formula is given as Z-Resolution = $(H_{h+}$ - $H_{h-})/h$ where H_{h+} and H_{h-} are the upper and lower interpolated points where the layer pixel sum reaches $\frac{1}{2}$ the maximum layer pixel sum and h is the cylinder height.

2.4. Human Volunteers: Method

In this experiment different postures were used to alter the angle at which the gravitational force acted on the lungs thereby causing changes in vertical distribution of ventilation. The distribution of ventilation depends strongly on gravity, such that, in normal spontaneously-breathing lungs, more ventilation occurs in dependent regions. This effect has been widely studied in supine subject (e.g. Frerichs *et al* 2001). It was thus expected that change in posture would alter the lung mechanics of a subject

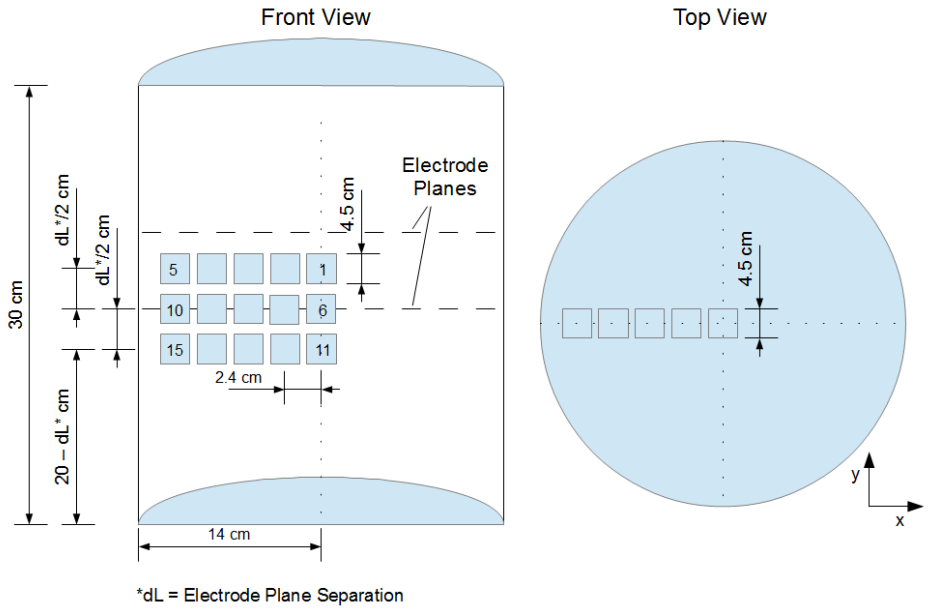

Figure 3: Block placement locations. Blocks are placed in 15 positions over 3 levels. The first five blocks are vertically centred midway between the electrode planes. Level separation is set at $dL/2$ cm, where dL is the distance between the Electrode Planes.

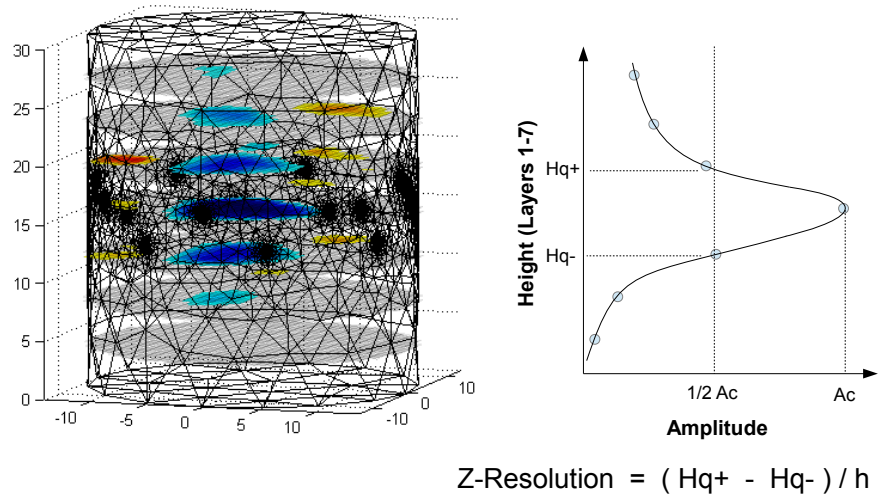

Figure 4: Z-Resolution is defined as the distance between H_{q+} and H_{q-}, which are the interpolated points where the Amplitude reaches $\frac{1}{2}$ the maximum value of the Amplitude at the block-centred plane, normalized by the cylinder height h. If the $\frac{1}{2}$ Amplitude is not met in one or both directions, the tank boundary is used.

such that the lung region of highest volume change would shift vertically according to posture.

This experiment was performed using eight healthy human subjects (approved by the Carleton University Research Ethics Board #100712). All subjects signed a Letter of Consent which permits the anonymous storage and publication of the gathered data. Exclusion criteria for subjects included any vascular or respiratory medical conditions, as well as habitual smoking. Subjects were male between the ages of 24 and 45. EIT and spirometry data from these experiments have been made available in "EIDORS Contributed Data" at `eidors.org`.

Each subject performed two tidal breaths followed by vital capacity (VC) breathing for a total of 60 seconds. During this time, 3D EIT and spirometry measurements were obtained simultaneously. The experiments were repeated with EIT measurements taken using the three measurement patterns selected according to the conclusions of the tank experiment. For each measurement pattern, the subject then performed the breathing protocol in the standing, sitting, supine, and head-down decline (35°) posture.

EIT data were acquired by placing 16 electrodes around the upper torso against the skin. The lower ring was placed 4 cm above the base of the sternum and the upper ring was placed 4 cm above the first ring. A ground electrode was placed under the ribcage on the front right side. EIT measurements were taken using the Goe-MF II EIT device and spirometry measurements were taken using the iWorx-214 spirometer and physiological data acquisition system. The data acquisition rate was set to 200 samples/second. Each individual EIT measurement frame was reconstructed onto an adult male thorax FEM using the 3D GREIT method with a noise figure of 0.5. The images from each set of measurement frames form a time series image set.

2.5. Human Volunteers: Analysis

EIT image sequences were compared with spirometry measurements for each subject and protocol to determine whether the EIT signal accurately captured global change in lung volume. The global EIT amplitude signal was calculated as the sum of the pixel amplitude of each EIT image to form a time series vector, and compared to the lung volume measurements from the spirometer.

Several signal conditioning steps were required. First, the acquisition rates differed by a factor of 16. A peak-matching algorithm was used to align the two signals, and the nearest spirometry data point timewise was taken to match each EIT data point. Second, the spirometry data showed significant drift. This was corrected by creating a 6th polynomial line matching the spirometry trend and then subtracting the polynomial line from the spirometry signal. Finally, the data representing the two tidal breaths were discarded so that only the VC breaths were considered in the analysis.

The global EIT amplitude signal was then compared to the spirometry data by calculating the correlation coefficient between the two data sets. The results were averaged over all subjects for each posture and for each EIT measurement pattern.

The EIT data were then compared to the spirometry data by calculating the Root Mean Square Error (RMSE) between the measurement sets. This gives an estimate of the error in the EIT signal in capturing the lung volume change in comparison with the spirometry method. The data were again averaged over all subjects for each posture and for each EIT measurement pattern.

In order to quantify the gravitational effects on vertical lung mechanics, functional EIT (fEIT) images were calculated. The approach of using fEIT images was based on the method described by Frerichs *et al* (2001) to analyze transthoracic gravitational effects in EIT imaging where a polynomial line was fit to the global EIT amplitude signal and the coefficients of the polynomial were used as features. An fEIT image therefore represents a specific feature of pixel behaviour over the time series image set.

Features were extracted from the inhalation curves in each image set. The inhalation curves were determined by segmenting the global EIT amplitude signal for each time series image set, where the maximum and minimum peaks in the signal corresponded to full inhalation and full exhalation respectively. The inhalation segment was selected as the data from a minimum to a maximum point in the global amplitude signal. Segments of less than half the maximum peak amplitude difference were discarded as a non-vital capacity breathing manouvre.

Four features were calculated for each image set: *f1* is the average minimum to maximum amplitude difference of the inhalation segments; *f2*, *f3* and *f4* are the average coefficients of a second order polynomial line fit to each inhalation segment. Four fEIT images were then produced for each image set.

The fEIT images were analyzed to determine whether difference in vertical regional activity could be distinguished between postures. For each fEIT image, the fraction of the total pixel amplitude of each layer l is calculated as $A_l = N_{q,l} / \sum N_{q,l}$ where $N_{q,l}$ is the number of pixels with value $\geq \frac{1}{4}$ of the maximum pixel value of the image for layer l. The Activity, A_l, (as %) is plotted against the reconstruction layer and the slope is calculated. The % Activity slope is then compared between postures.

3. Results

3.1. Tank Measurements

The measurements recorded in the tank phantom experiment were reconstructed using the 3D GREIT method. The reconstructed images were then analyzed using GREIT FoM and the Z-Resolution measure. The PP and ZP patterns produced noisy images which did not show the reconstructed block and are therefore not included in the results. This corresponds with the simulation results.

Figure 5 shows the reconstructed images for the first 5 block positions on the centre plane with a plane separation of 3.2 cm. Image characteristics are similar on the lower block layers (2 and 3). The PL, PO, ZZ and SQ patterns showed a poor ability to discern object edges in the z-direction, especially at the centre of the cylinder where the

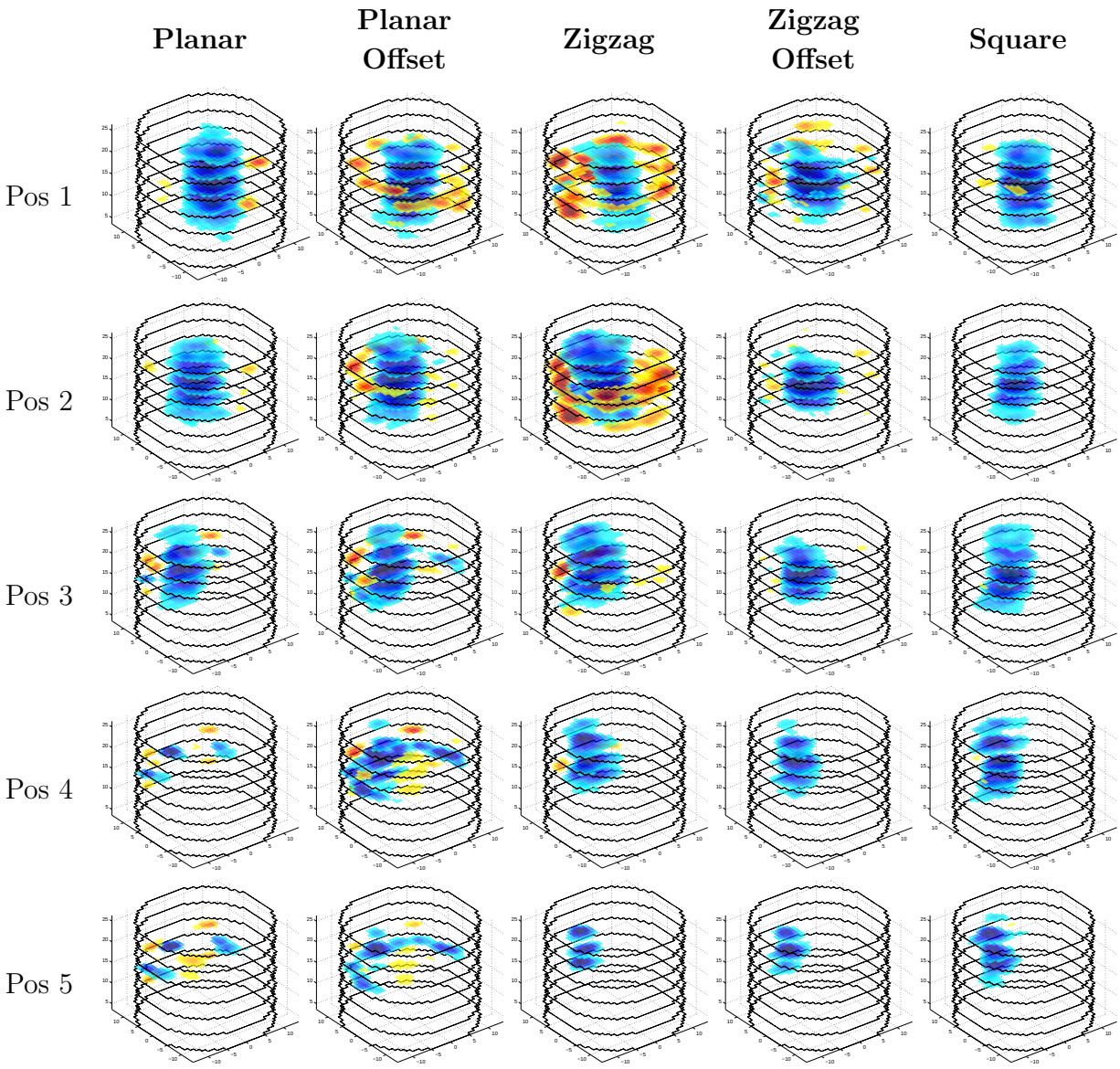

Figure 5: Reconstructed images of a block in 5 positions on the centre plane of a cylindrical tank. Measurements taken using Planar (PL), Planar Offset (PO), Zigzag (ZZ), Zigzag Offset (ZO) and Square (SQ).

reconstructed blocks stretch across the full axis of the cylinder. Close to the edge of the cylinder, the block images were better resolved. However, the PL and PO patterns compressed the object to a single plane and there is a spreading along the cylinder edge which degrades the planar resolution. The ZO pattern had the best resolution on the z-axis. However, several artifacts can be seen when the object is on the plane furthest from the centre. When the electrode plane separation was increased to 7.1 cm, the overall quality of the ZZ, ZO, and SQ patterns degraded while the quality of the PL and PO patterns was more consistent.

The results for the Amplitude, Position Error, and Resolution FoM and the Z-

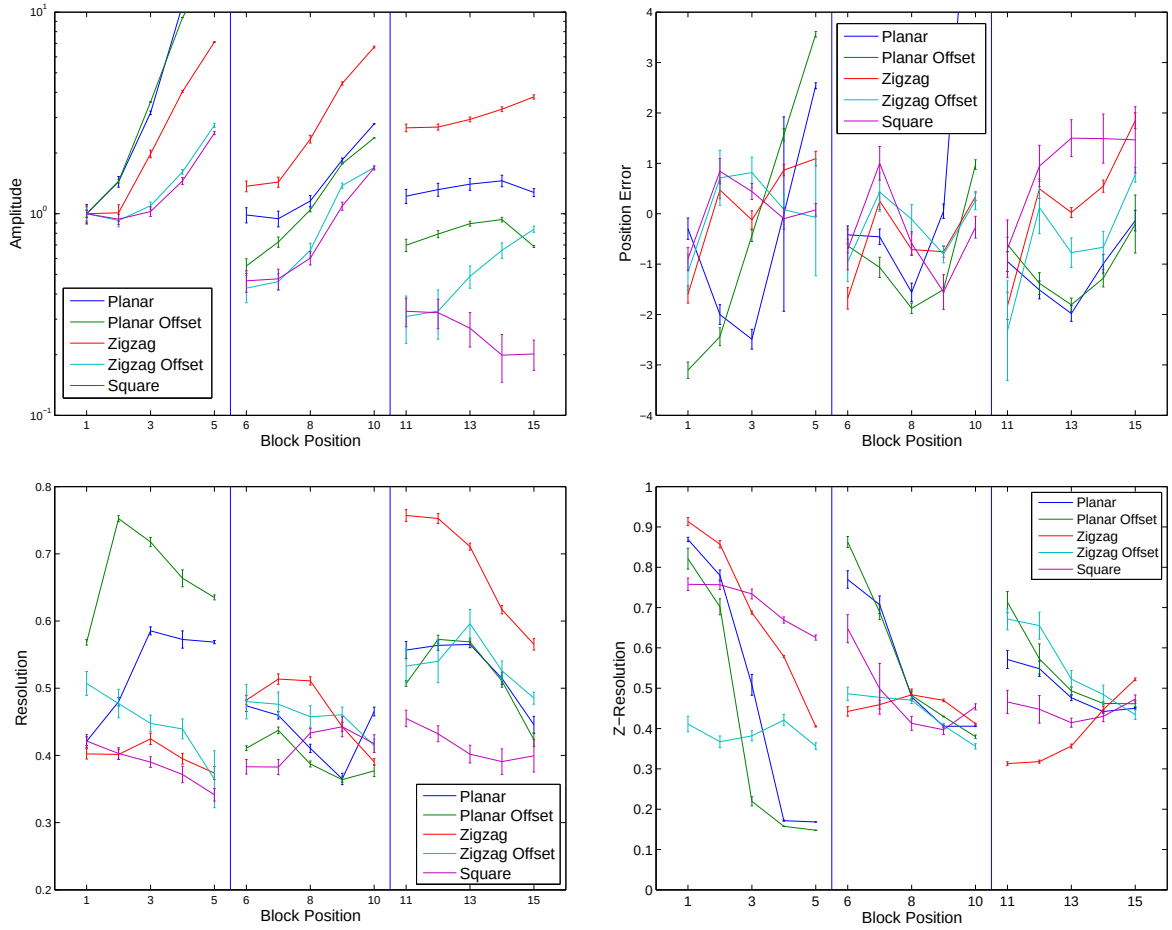

Figure 6: Results for five 3D measurement pattern performance for Amplitude (top left), Position Error (top right), Resolution (bottom left), and Z-Resolution (bottom right). Amplitude units in ω/m and Position Error units in cm.

Resolution measure are shown in figure 6. In an ideal algorithm, the amplitude response would remain consistent over the radius of the cylinder; however, all patterns showed some increase toward the boundary. The PL, PO and ZZ patterns showed significant increase moving towards the edge, while the ZO and SQ patterns had better performance with more consistent Amplitude over the cylinder radius.

The Position Error is defined such that a positive value indicates an image was closer to the centre than the true position; an ideal algorithm would yield position errors of zero. The observed performance was quite consistent among of all patterns. Results were similar with PL and PO having the largest Position Error on the centre plane. The ZZ, ZO, and SQ patterns showed more stable and consistent Position Error across the cylinder radius.

The desired performance for Resolution was a low value. Most patterns showed improvement in Resolution moving towards the edge of the cylinder. The SQ pattern had the lowest Resolution on layer 1 but had higher values along with ZZ layers 2 and

3. The PL and ZO patterns had the most consistent Resolution over all three layers.

The desired response for the Z-Resolution was a low and consistent value for all object positions. The ZO pattern was observed to give a low, consistent value for positions 1–10. The PL and PO patterns typically had poor performance in the centre but high performance at the edge, which is where the compressing and spreading effects were seen in the images.

3.2. Human Volunteers

First, global EIT signals were compared to the values from spirometry. The results for the correlation and RMSE analysis of the global EIT amplitude vs. spirometry signals are shown in figure 7. A summary for each pattern is given in Table 1. Overall, the results show a strong correlation of EIT values with those of spirometry, with only Subject 3 and Subject 7 having a value lower than 0.75. The average pattern correlation ranged from 0.840 for PL to 0.898 for SQ. Similarly RMSE values were typically below 0.2 with the average pattern RMSE ranging from 0.169 for PL to 0.145 for SQ. The PL pattern had the poorest performance for both correlation and RMSE but the difference was not statistically significant. The high correlation and low RMSE between the two data sets suggests that 3D EIT images generated using the 3D GREIT algorithm are capable of accurately measuring changes in lung volume.

Several data sets were not included in the results. A number of spirometry data sets had high drift, and useable results were retrieved where possible using a higher order polynomial (12) . Subject 7-ZO-Decline and Subject 5-PL-Sitting were discarded for this reason. In addition there was no data for Subject 3-Decline due to equipment unavailability.

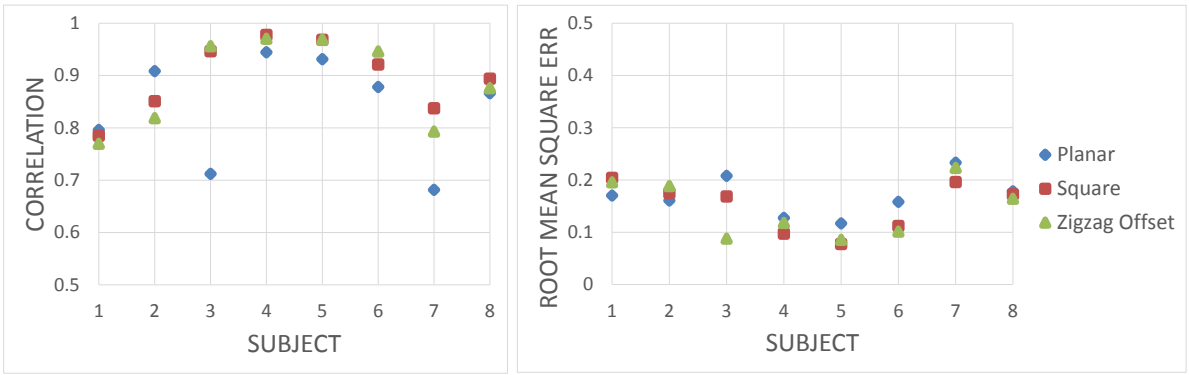

Figure 7: The correlation (left) and root mean square error (right) between global EIT amplitude and spirometry lung volume for each subject averaged across all 4 postures. Average correlation for all subjects is shown in the table for each measurement pattern.

Four fEIT images were generated for each subject, measurement pattern, and posture. The images represent regional lung activity based on the feature used to generate the image. The fEIT images were analyzed by layer in order to quantify

Table 1: Summary of Correlation results by pattern.

Parameter	**Planar**	**Zigzag Offset**	**Square**
Mean Correlation	0.840	0.887	0.898
Std. Dev.	0.139	0.110	0.088
Average RMSE	0.169	0.150	0.145
Std. Dev.	0.038	0.048	0.054

changes in vertical lung activity. Figure **??** shows fEIT representative images from two different subjects generated using *f2*. Sagittal cut planes through the centre of the left and right halves of the thorax, as described in Figure **??**, were isolated to show differences in vertical lung activity. The images presented well-defined lung regions, however, significant differences in vertical lung activity were not directly observable for different postures.

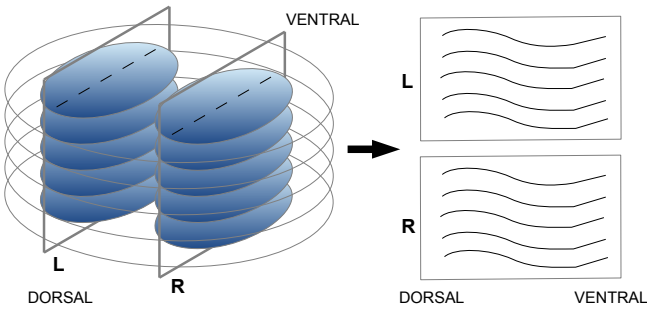

Figure 8: Schematic diagram of the representation of 3D lung EIT images, showing sagittal cutplanes of pixel amplitude values are selected from fEIT images on the centre of the left and right halves of the thorax to show vertical lung behaviour.

In order to detect change in vertical lung activity due to a change in posture, the %Activity was calculated for each image layer and a linear line was fit to the %Activity vs. layer data. The slope of the line was then plotted against posture for each feature and measurement pattern. Figure **??** shows %Activity slope vs. posture results averaged over all subjects.

A paired t-test was used to analyze the statistical significance of variation in the %Activity slope between different postures. This paired t-test used the null-hypothesis that the %Activity slope results for all subjects for two different postures were from the same parent distribution, and determined whether the null-hypothesis could be rejected given a significance level of 5%. The t-test was performed by comparing the %Activity slope results each of the decline, supine, and sitting posture results to the standing posture. Table 2 shows the results for the 4 fEIT images for each measurement pattern.

The results of the t-test showed seven cases (*) with statistical significance. For the SQ pattern, the %Activity slope results for the decline and sitting postures were

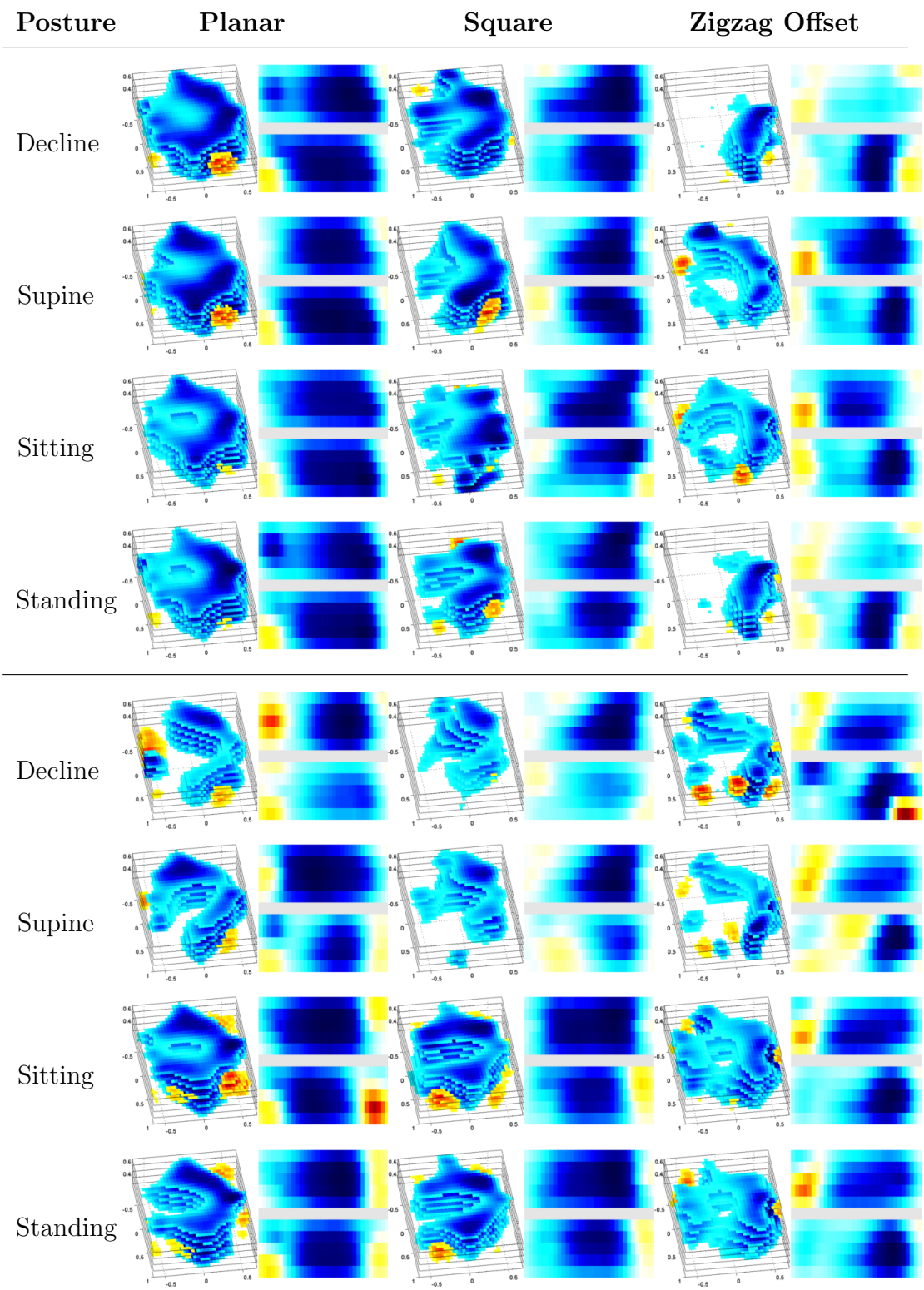

Figure 9: Functional EIT images for Subjects 2 (above) and 8 (below) which have been generated using feature 2 for the Planar, Square, and Zigzag Offset measurement patterns and 4 postures. A full fEIT image (left) is shown comprised of axial slices and sagittal cutplanes are shown centred on the left lung (right above) and right lung (right below). A description of image orientation is shown in Figure **??**.

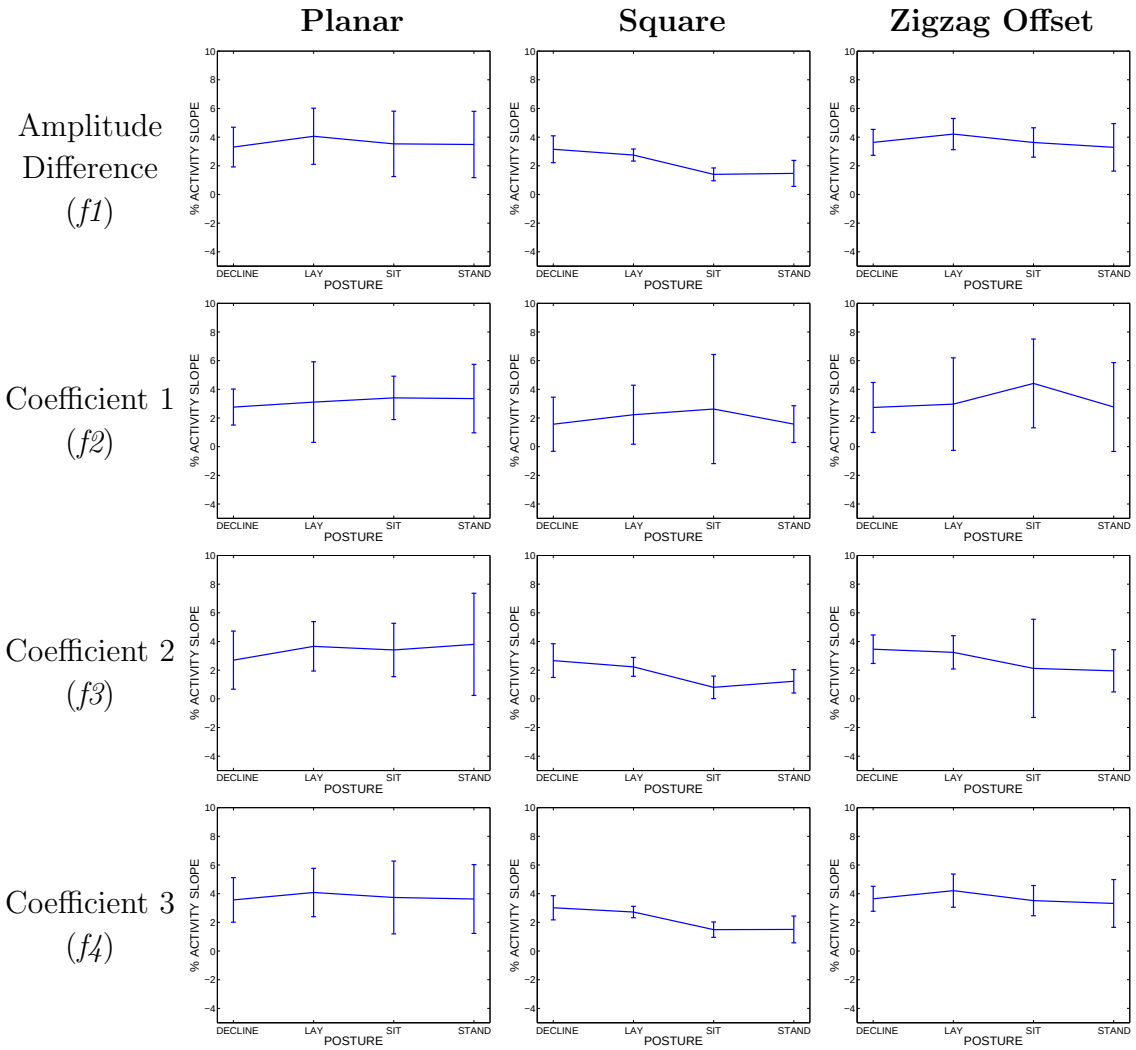

Figure 10: A set of graphs of %Activity Slope vs. Posture averaged over all eight subjects. Postures include decline, supine (lay), sitting, and standing. Results are shown for the Planar, Zigzag Offset, and Square patterns and for all four features.

Table 2: The p-value results of paired t-test comparing %Activity slope values between postures. The significance is set to 5%.

p-values	**Planar**			**Square**			**Zigzag Offset**		
features	Dec	Sup	Sit	Dec	Sup	Sit	Dec	Sup	Sit
f1	0.845	0.533	0.874	0.011*	0.002*	0.863	0.608	0.230	0.616
f2	0.557	0.866	0.956	0.994	0.382	0.351	0.981	0.920	0.184
f3	0.219	0.907	0.676	0.036*	0.016*	0.308	0.034*	0.091	0.915
f4	0.948	0.629	0.645	0.019*	0.002*	0.976	0.618	0.239	0.780

statistically different than that of the standing posture for features 1, 3 and 4. The ZO pattern showed statistically significant differences in %Activity slope for feature 3 for the decline vs. standing comparison. The PL pattern did not show any significant results.

4. Discussion

Since electrical current propagates diffusely, image reconstruction in EIT is inherently 3D. While it has been common to reconstruct a 2D "slice" from a single plane of electrodes, such a slice is sensitive to a large volume. The promise of 3D EIT is to distinguish such volumetric regions. By using at least two planes of electrodes, stimulation and measurement patterns are used which are sensitive to both in- and out-of-plane effects. However, the possible choices for such patterns are large, so it is necessary to understand the relative benefits. Since previous work has compared stimulation and measurement patterns via simulation, our goal in this paper is to evaluate these results in phantom and human volunteer experiments.

The results of the phantom experiment and the volunteer measurements indicate that, while 3D EIT using two electrode layers does provide useful 3D images in terms of capturing conductivity contrasts and global change in lung volume, the approach is not sufficient in detecting regional changes in conductivity in a 3D region. The images from the phantom experiment show reasonable Resolution and Position Error in the xy plane. However, the image is poorly constrained along the z-axis leading to poor Z-Resolution with the Zigzag Offset pattern showing the best performance. Similarities in performance results between patterns suggest that the ratio of horizontal to vertical electrode pairs in a measurement pattern has an effect on image quality, particularly for Position Error and Z-Resolution.

The fEIT images from the human subjects showed significant differences in the vertical distribution of lung activity as posture changed. The effect was strongest (most significant) for the Square pattern. However, the there was no pattern which was "best" for all subjects and all postures.

Based on our results, we feel able to make several recommendations for the selection of stimulation and measurement patterns for 3D EIT using two rings of electrodes. First, the opposite patterns (PP and ZP) do not perform well. We interpret this result as a consequence of the loss of information in an opposite stimulation (a two-fold redundancy is introduced for both stimulation and measurement). Of the remaining patterns, there does not appear to be much difference between placement of electrodes in vertical columns and offset placements. Since placement in vertical columns is practically easier, we recommend against using offset placements. This leaves the Planar, Zigzag and Square patterns. Based on our phantom results, the Zigzag has the best vertical resolution, followed by Square and Planar. This effect can be explained by the larger number of measurements with a vertical component in the Zigzag (followed by the Square, with much less vertical component for the Planar). On the other hand, for the

in-plane resolutions the worst performer was Zigzag, which has no in-plane measurement components. We judge the overall best performance to be the Square pattern, which had the best and most uniform in-plane resolution, the most uniform amplitude response, and an average vertical resolution.

Of the three patterns chosen for human volunteer measurements (Planar, Square and Zigzag), we observed fair performance in all cases. It was possible to create EIT lung images in which the two lungs were clearly separable in all cases. For the vertical resolution, the physiological changes we expected were relatively subtle (change of vertical distribution of ventilation with posture). This effect is statistically significant in more than one case only for the Square pattern, and the images (figure **??**) also appear to show a convincing vertical aeration change only for the Square pattern.

There are several limitations to our study: first, we considered only sixteen-electrode pair-drive EIT systems. While 16 electrodes may provide adequate resolution for a single plane, the requirement to distribute the electrodes over two planes is somewhat limiting, and additional electrodes and electrode planes are required for improved detection of regional inhomogenieities in 3D space. Another limitation is that only a limited set of stimulation and measurement patterns were explored for phantom and human volunteer tests. A larger set could be explored in the initial simulation phase since the total space of patterns is large and it is possible that patterns not selected could outperform the ones that were tested. Finally, the selection of posture variations as a technique to provoke vertical redistributions of aeration has its limitations. The extent of the redistribution is not well known, and no gold standard measure was used to validate the size of the changes. Nevertheless, gravity-dependent aeration changes are a well documented physiological phenomenon, and our statistical test are expected to show convergent validity.

This paper explores the benefits of using two rings of electrodes for EIT imaging of the lungs. For both tank and human volunteer studies, the results show that image reconstruction performance is strongly affected by the choice of stimulation and measurement pattern. For the vertical resolution, the Zigzag patterns were best, but for a good overall performance, our recommendation is the Square pattern.

References

Adler A and Lionheart W R B 2006 Uses and abuses of EIDORS: An extensible software base for EIT *Physiol Meas* 27 S25–S42

Adler A Arnold JH Bayford R Borsic A Brown B Dixon P Faes TJC Frerics I Gagnon H Gärber Y Grychtol B Hahn G Lionheart WRB Malik A Patterson RP Stocks J 2009 GREIT: a unified approach to 2D linear EIT reconstruction of lung images *Physiol Meas* 30(6) S35–55

Adler A Gaggero P O Maimaitijiang Y 2011 Adjacent stimulation and measurement patterns considered harmful *Physiol Meas* 32(7) S731–S744

Adler A Amato MB Arnold JH Bayford R Bodenstein M Böhm SH Brown BH Frerichs I Stenqvist O Weiler N Wolf GK 2012 Whither lung EIT: where are we, where do we want to go and what do we need to get there? *Physiol Meas* 33 679–94

Adler A, Frerichs I Grychtol B 2015 The off-plane sensitivity of EIT *Proc. EIT 2015*, p 68, Neuchâtel, Switzerland, Jun 2–5, 2015

Dehghani H, Soni N, Halter R, Hartov A & Paulsen K D 2005 Excitation patterns in three-dimensional electrical impedance tomography *Physiol Meas* 26(2) S185–S197

Fabrizi L, McEwan A, Oh T, Woo E J & Holder D S 2009 An electrode addressing protocol for imaging brain function with electrical impedance tomography using a 16-channel semi-parallel system *Physiol Meas* 30() S85–S101

Frerichs I, Dargaville P A & Rimensberger P C 2013 Regional respiratory inflation and deflation pressure-volume curves determined by electrical impedance tomography *Physiol Meas* 34 567–577

Frerichs I Dudykevych T Hinz J Bodenstein M Hahn G Hellige G 2001 Gravity effects on regional lung ventilation determined by functional EIT during parabolic flights *Journal of Applied Physiology* 91(1) 39–50

Graham B & Adler A 2007 Electrode Placement Configurations for 3D EIT *Physiol Meas* 28 (7) S29–44

Grychtol B Müller B Adler A 2015 3D EIT image reconstruction with GREIT. *Proc. EIT 2015*, p 27, Neuchâtel, Switzerland, Jun 2–5, 2015

Kantartzis P, Abdi M & Liatsis P 2013 Stimulation and measurement patterns versus prior information for fast 3D EIT: A breast screening case study *Signal Processing* 93(10) 2838-2850

Kirby M Mathew L Heydarian M Etemad-Rezai R McCormack DG Parraga G 2011 Chronic Obstructive Pulmonary Disease: Quantification of Bronchodilator Effects by Using Hyperpolarized He MR Imaging *Radiology* 261 283–293

Mamatjan Y, Gursoy D & Adler A 2011 Electrode positions and current patterns for 3D EIT Conf EIT 2011 Bath, UK

Metherall P, Barber D C, Smallwood R H & Brown B H 1996 Three-dimensional electrical impedance tomography *Nature* 380 509–512

Polydorides N & Lionheart W R B 2002 A Matlab toolkit for three-dimensional electrical impedance tomography: a contribution to the Electrical Impedance and Diffuse Optical Reconstruction Software project *Measurement Science and Technology* 13 1871–1883

Putensen C, Zinserling J, Wrigge H 2006 Electrical Impedance Tomography for Monitoring of Regional Ventilation in Critically III Patients in *Int Care Med* 448-457 Springer New York 448–457

Stephenson D R Davidson J L Lionheart W R H Grieve B D York T A 2005 Comparison of 3D Image Reconstruction Techniques using Real Electrical Impedance Measurement Data *4th World Congress on Industrial Process Tomography* Aizu, Japan

Wagenaar J Grychtol B & Adler A 2014 An Approach to Extend GREIT Image Reconstruction to 3D *Conf EIT 2014* Gananoque, Canada

Wagenaar J 2015 *Electrical Impedance Tomography in 3D: characterization and evaluation*, M.A.Sc., Carleton University.

Wolf G K Gomez-Laberge C Kheir J N Zurakowski D Walsh B Adler A Arnold J H 2012 Reversal of dependent lung collapse predicts response to lung recruitment in children with early acute lung injury. *Pediatric Critical Care Medicine* 13 (5) 509–515

Zhao Z Fischer R Frerichs I Muller-Lisse U Moller K 2012 Regional ventilation in cystic fibrosis is measured by electrical impedance tomography. *Journal of Cystic Fibrosis* 11 412–418